

Solar wind-magnetosphere-ionosphere coupling and its impact on equatorial ionospheric electrodynamics during the 23 March 2023 geomagnetic storm: Effect of sudden decrease of solar wind dynamic pressure

Guan Le¹, Guiping Liu¹, Endawoke Yizengaw², Chin-Chun Wu³, Yihua Zheng¹, Sarah Kimberly Vines⁴, and Natalia Buzulukova⁵

¹NASA Goddard Space Flight Center

²The Aerospace Corporation

³Naval Research Laboratory

⁴Johns Hopkins University Applied Physics Laboratory

⁵UMCP/NASA GSFC

April 12, 2024

Abstract

We present a study of the magnetosphere-ionosphere coupling during the 23 March 2023 magnetic storm, focusing on the effect of the drastic decrease of the solar wind dynamic pressure occurred during the main phase. Our observations show that the negative pressure pulse had significant impact to the magnetosphere-ionosphere system. It weakened large-scale field-aligned currents and paused the progression of the storm main phase for ~3 hrs. Due to the sudden decrease of the plasma convection after the negative pressure pulse, the low-latitude ionosphere was over-shielded and experienced a brief period of westward penetration electric field, which reversed the direction of the equatorial electrojet. The counter electrojet was observed both in space and on the ground. A transient, localized enhancement of downward field-aligned current was observed near dawn, consistent with the mechanism for transmitting MHD disturbances from magnetosphere to the ionosphere after the negative pressure pulse.

**Solar wind-magnetosphere-ionosphere coupling and its impact on equatorial
ionospheric electrodynamics during the 23 March 2023 geomagnetic storm:
Effect of sudden decrease of solar wind dynamic pressure**

Guan Le¹, Guiping Liu¹, and Endawoke Yizengaw², Chin-Chun Wu³, Yihua Zheng¹, Sarah Vines^{4,5},
Natalia Buzulukova^{1,6}

¹NASA Goddard Space Flight Center, Greenbelt, MD (guan.le@nasa.gov)

²The Aerospace Corporation, El Segundo, CA

³Naval Research Laboratory, Washington, DC

⁴Applied Physics Laboratory, Laurel, MD

⁵Now at Southwest Research Institute, San Antonio, TX

⁶University of Maryland, College Park, MD

Corresponding author: Guan Le (guan.le@nasa.gov)

Key Points:

1. Direct evidence of prompt penetration of electric field in the equatorial ionosphere caused by negative solar wind pressure pulse
2. Transient counter electrojet caused by westward penetration electric field after the arrival of negative pressure pulse
3. Significant decrease of global large-scale FACs and transient enhancement of localized FAC in response to negative pressure pulse

Abstract

We present a study of the magnetosphere-ionosphere coupling during the 23 March 2023 magnetic storm, focusing on the effect of the drastic decrease of the solar wind dynamic pressure occurred during the main phase. Our observations show that the negative pressure pulse had significant impact to the magnetosphere-ionosphere system. It weakened large-scale field-aligned currents and paused the progression of the storm main phase for ~ 3 hrs. Due to the sudden decrease of the plasma convection after the negative pressure pulse, the low-latitude ionosphere was over-shielded and experienced a brief period of westward penetration electric field, which reversed the direction of the equatorial electrojet. The counter electrojet was observed both in space and on the ground. A transient, localized enhancement of downward field-aligned current was observed near dawn, consistent with the mechanism for transmitting MHD disturbances from magnetosphere to the ionosphere after the negative pressure pulse.

Plain Language Summary

The solar wind is a continuous stream of charged particles blowing from the Sun. The Earth's magnetic field forms a protective shield around our planet, called the magnetosphere, which deflects most of the solar wind particles away from the Earth. Disturbances in the solar wind can interact with the magnetosphere and impact the Earth's upper atmosphere (ionosphere). The interaction creates electric fields forcing charged particles to move in the magnetosphere, which creates electric currents flowing along the magnetic field lines connecting to the high-latitude ionosphere and drives the movement of charged particles there. The low-latitude ionosphere is generally shielded from these electric fields. Sudden changes in the solar wind can break such balance, leading to the electric field penetration to low latitudes. We examined how the magnetosphere and ionosphere interacted during the 23 March 2023 geomagnetic storm, focusing on what happened when the solar wind dynamic pressure suddenly decreased. We found the pressure drop caused a sudden decrease of the high-latitude electric field, resulting in a brief period of overshielding and the electric field in the equatorial ionosphere reversed its direction. This changed the direction of the equatorial electrojet, a major electric current in the ionosphere at the magnetic equator.

1 Introduction

In steady-state conditions, the low-latitude ionosphere is shielded from the high-latitude convection electric field due to the partial ring current-associated region-2 (R2) field-aligned currents (FACs) which act to oppose the electric field associated with region-1 (R1) FACs (e.g., Southwood, 1977). However, it can be directly coupled to the magnetospheric disturbances through prompt penetration of the convection electric field during active times (Nishida, 1968; Jaggi and Wolf, 1973; Fejer et al., 1979).

The equatorial electrojet (EEJ), an intense band of eastward electric current flowing along the dayside magnetic equator in the E-region ionosphere (~ 110 km altitude), is driven by an eastward zonal electric field from plasma-neutral collisional interactions known as the E-region wind dynamo (Richmond, 1973; Heelis, 2004). The intensity and polarity of the EEJ respond directly to the perturbations of the zonal electric field. Variations of the EEJ often serve as an indicator for the equatorial zonal electric field perturbations, which can be caused by either neutral wind changes from lower atmosphere forcing or prompt penetration electric fields (PPEFs) from enhanced magnetosphere-ionosphere (M-I) coupling. Many studies have used EEJ variations to probe the presence of PPEFs that are attributed to interplanetary magnetic field (IMF) variations (e.g., Yizengaw et al., 2011, 2016) or solar wind dynamic pressure pulses (e.g., Nilam et al., 2020, 2023). Understanding the sources and the process of PPEFs continues to be a subject of ongoing investigation (Kelly et al., 2003; Fejer et al., 2024).

This paper reports the observations of the M-I coupling and its effect on the equatorial ionosphere in response to a sudden decrease of the solar wind dynamic pressure during the main phase of the 23 March 2023 geomagnetic storm. Figure 1 shows 1-min resolution OMNI data for the IMF and solar wind parameters along with ground-based SYM-H index for 23-25 March 2023. This large storm (minimum Dst ~ -170 nT, Kp ~ 7) was associated with the passage of an interplanetary coronal mass ejection (ICME), triggered by the southward IMF in both the sheath and the ICME regions. A drastic density decrease was observed at the boundary crossing from the sheath to the ICME by the WIND spacecraft. As a result, a significant negative solar wind pressure pulse hit the

Earth's magnetosphere during the main phase of the storm (1440 UT, marked by the red dashed line in Figure 1). The solar wind density as well as the dynamic pressure decreased by a factor of ~ 10 .

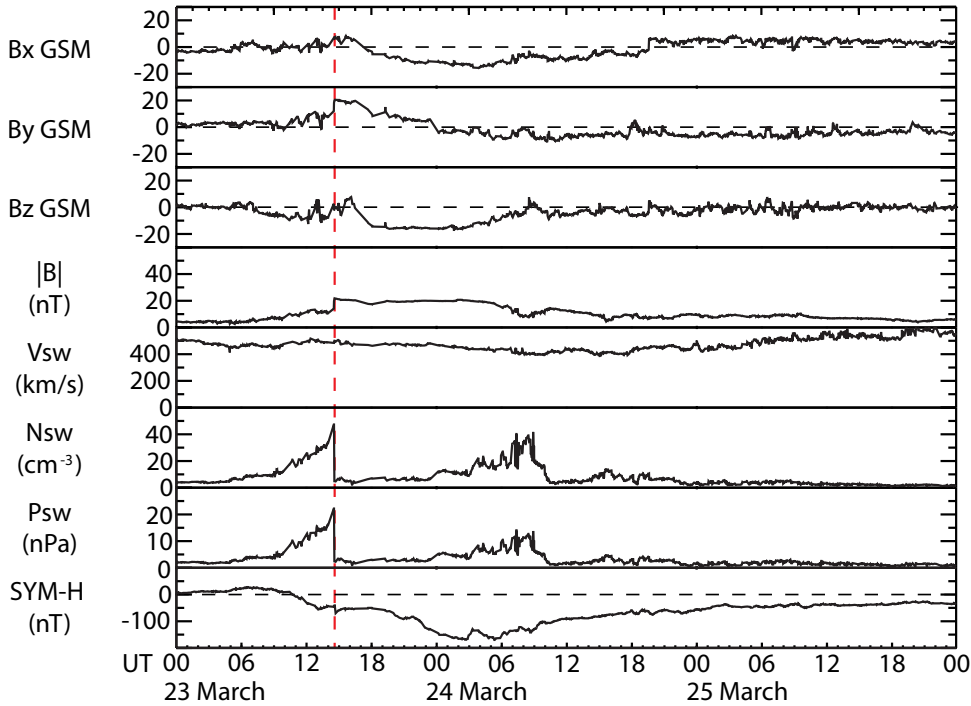


Figure 1. The 1-min resolution OMNI data with IMF/solar wind parameters (top 7 panels) and SYM-H index (bottom panel) for 23 March 2023 magnetic storm. The negative pressure pulse during the main phase of the storm is marked by the red dashed line.

We examine how FACs at high latitudes and the EEJ at the equator responded to the negative pressure pulse using both space and ground-based magnetic field data. In the following sections, we first present evidence for a transient PPEF associated with the pressure pulse from the ground based EEJ observations. Then we examine the response of large-scale FACs globally by AMPERE and locally by Swarm satellites. We also analyze the EEJ observations in space by Swarm, which provide additional evidence for the transient PPEF associated with the pressure pulse. Finally, we discuss the dynamic processes involving solar wind pressure pulse interacting with the magnetosphere and coupling into the polar ionosphere, that allow us to understand the behaviors of the equatorial ionosphere.

2 Observations

2.1 Ground-based Observations of the EEJ

The EEJ signals can be obtained from a pair of ground magnetometer stations located near the magnetic equator on the same meridian, one directly under the EEJ at the equator (within $\pm 3.5^\circ$) and the other just off the EEJ region (6° – 9° from the magnetic equator) (Anderson et al., 2004; Yizengaw et al., 2014). The EEJ signals can only be detected by the station at the magnetic equator because the EEJ current is confined in a narrow latitudinal band (within $\pm 3^\circ$). But both stations are expected to record the same magnetic field variations from other large-scale current sources, such as the solar quiet (Sq) currents, the ring current, and the magnetopause current. The EEJ signals are extracted from the difference of the H-components between the two stations. In this study, we used two pairs of geomagnetic observatories at two meridians ($\sim 80^\circ\text{W}$ and $\sim 50^\circ\text{W}$). One pair is located at Jicamarca (JICA, $11.95^\circ\text{S}/76.87^\circ\text{W}$ GEO, $\text{MLat} = 0.6^\circ\text{N}$) and Piura (PIUR, $5.2^\circ\text{S}/80.6^\circ\text{W}$ GEO, $\text{MLat} = 6.9^\circ\text{N}$) in Peru. The other pair is located at Tatuoca, Brazil (TTB, $1.21^\circ\text{S}/48.5^\circ\text{W}$ GEO) and Kourou, French Guyana (KOU, $5.21^\circ\text{N}/52.7^\circ\text{W}$ GEO). TTB and KOU are well located under and far enough from the EEJ, respectively. They are within the region of South Atlantic Anomaly with rapid northward moving of the magnetic equator, and the magnetic equator passed the TTB in March 2013 (Morschhauser et al., 2017).

Figure 2 shows the magnetic field observations from the 2 pairs of ground observatories on 23 March 2023 with three subpanels for each pair, from top to bottom, showing the H-component with the background removed (δH) off the magnetic equator, at the magnetic equator, and the EEJ signal (δH_{EEJ} , the differences between δH at the geomagnetic equator and off the equator), respectively. The horizontal bar in the 3rd subpanel indicates dayside hours (6–18 LT) at the equator station. The red dashed line indicates the time of the negative pressure pulse (1440 UT) in Figure 1. The local time (LT) of the pressure pulses at the two equator stations are also noted in Figure 2.

The eastward zonal electric field from the wind dynamo drives the eastward EEJ, producing a positive magnetic field perturbation ($\delta H_{EEJ} > 0$) in the dayside. This is generally the case in Figure 2 except for a brief period immediately following the negative pressure pulse. There was a transient negative impulse of the H-component at all the stations, consisting of a sharp decrease (~ 6 min) and

a relatively gradual (~ 1 hour) return, apparently due to the sudden decrease of the magnetopause current and expansion of the magnetosphere in response to the negative pressure pulse (Araki and Nagano, 1988). However, the transient negative impulse at the equator station is much stronger than its off-equator counterpart, and the EEJ signature reversed its sign showing a transient counter electrojet flowing westward. This observation indicates the negative pressure pulse set up a transient westward electric field (~ 1 hour) in the equatorial ionosphere.

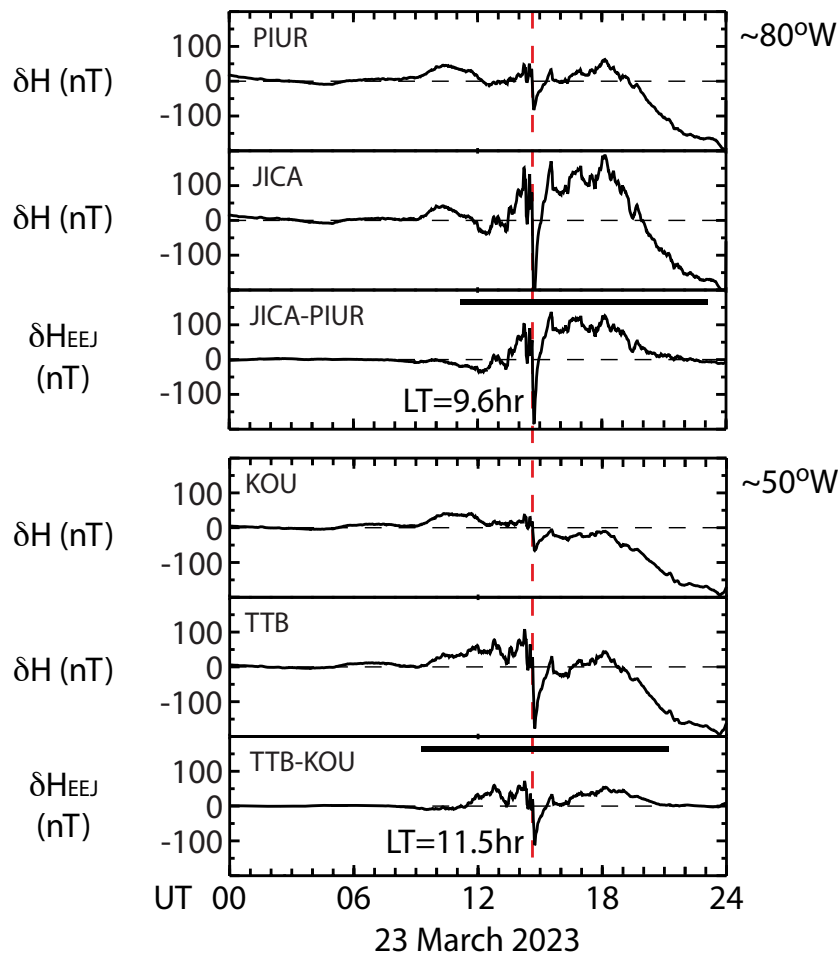


Figure 2. Ground-based observations of the H-component from 2 pairs of ground observatories on 23 March 2023, JICA-PIUR and TTB-KOU, respectively. The red dashed line marks the negative pressure pulse in Figure 1. The black horizontal bars indicate the daytime (06-16 LT) at the equator stations.

2.2 AMPERE Observations of Large-scale FACs

AMPERE observations of large-scale FACs are derived from global measurements of magnetic field perturbations from the Iridium constellation of more than 70 near-polar orbiting satellites [Anderson et al., 2000]. It collects 10-min data to generate one global pattern of large-scale FAC distributions and provides a continuous monitor of the state of the global M-I system. (AMPERE data will unlikely reveal transient and localized variations due to the limitation of spatial and temporal resolution.) Figure 3 shows the AMPERE observations of the total field-aligned currents flowing into and out of the ionosphere on 23 March 2023 (Figure S1 provides the magnetic field perturbations and global FAC maps). The total upward current out of one hemisphere is calculated by integrating all the upward current density over the entire area above 40° latitude, and likewise for the total downward current. Again, the red dashed vertical line corresponds to the negative pressure pulse in Figure 1.

Starting from ~ 07 UT, the total FACs gradually intensified as the storm progressed with the SYM-H index became more negative, representing an increasing active magnetosphere as FACs facilitate the electromagnetic energy input from the magnetosphere into the ionosphere. There is a brief period (~ 1 hr) of total current drop starting at ~13 UT, apparently associated with the northward excursion of the IMF Bz component (Figure 1) which turned off the dayside reconnection and reduced the magnetospheric convection temporally.

Figure 3 shows the total currents responded to the negative pressure in two stages. The total currents dropped sharply at ~1440 UT due to the sudden sunward motion of the magnetopause and expansion of the magnetosphere. The sudden reduction of the magnetopause current also caused a step decrease of the SYM-H index (Figure 1). Then the total currents continued to decrease gradually. The decreasing trend of the SYM-H index has flattened out within the storm main phase, indicating the pause of the ring current development (Figure 1). This is expected as IMF Bz fluctuated around zero and the expanded magnetosphere adjusted to the new state of reduced geomagnetic activity level. At ~1630 UT, the IMF Bz gradually turned southward, which terminated the decreasing trend of the total currents. At ~ 18 UT, both the total currents (Figure 3) and the SYM-H index (Figure 1) showed that the magnetospheric activities began to intensify

rapidly with the prolonged steady southward IMF in the ICME. In summary of the AMPERE observations, large-scale FACs were significantly weakened by the negative pressure pulse.

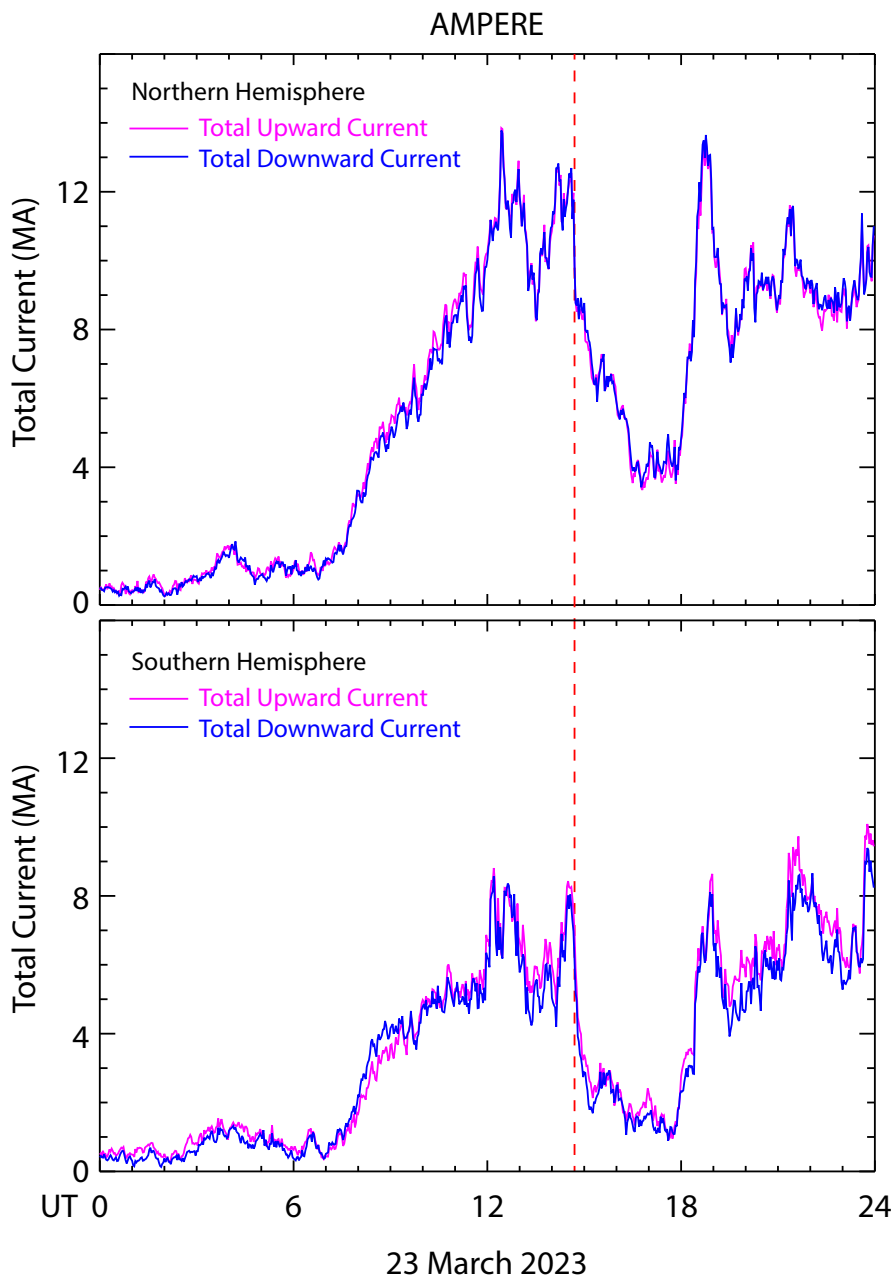


Figure 3. AMPERE Observations of the total amount of upward and downward FACs in northern and southern hemisphere, respectively.

2.3 Swarm Observations of FACs and EEJ

Swarm is a three-satellite mission in a high-inclination (87.5°) low-Earth orbit, which provides vector magnetic field data for frequent in situ measurements of FACs at high latitudes (Lühr et al., 2015) and scale magnetic field strength for the EEJ in the equatorial region (Alken et al., 2015). Among the three satellites, A and C form a pair flying side by side at the same altitude (~ 460 km) with a longitudinal separation of 1.4° . Swarm B has slightly higher altitude (~ 530 km) and its orbital plane slowly drifts apart from those of Swarm A/C. In this study, we used two official Swarm level-2 data products: (1) the vector magnetic field residuals $\delta \mathbf{B}$ for the study of FACs, and (2) the height-integrated latitudinal profile of eastward EEJ current. The EEJ current profile is estimated from the Swarm scalar magnetic field measurements by isolating the EEJ signal from the many other geomagnetic sources and then fitting the EEJ signal with a line current model (Alken et al., 2015). The EEJ current peak at the magnetic equator provides a good estimate of the EEJ strength.

Figure 4 presents an overview of the Swarm observations. Figure 4a shows the spacecraft orbits for the polar cap pass near 1440 UT, the intervals marked by the red bars in Figures 4b/4c. Figures 4b and 4c contain 4 hours of Swarm vector magnetic field residuals $\delta \mathbf{B}$ in solar magnetic (SM) coordinate system centered at 1440 UT (red dashed line) for Swarm A and B, respectively. Swarm C data are nearly the same as Swarm A (not shown). During this interval, Swarm made 5 passes of the polar cap, denoted by N (S) for the northern (southern) hemisphere, and 3 crossings of the dayside magnetic equator marked by MEq and the blue dashed lines. The perturbations in $\delta \mathbf{B}$ are the signals of FACs, occurring at auroral latitudes on both sides of the magnetic pole. The latitudinal profiles of the estimated EEJ current at the dayside magnetic equator crossings are presented in Figures 4d-4f for Swarm A and 4g-4i for Swarm B. The positive current is for eastward EEJ.

Both Swarm A and B were in the dayside morning sector over the northern polar cap at the time of the negative pressure pulse (red dots in Figure 4a). In Figure 4a, the tick marks on each trajectory are separated by 10 min. The red arrows indicate the directions of the spacecraft motion. Swarm A was moving from nightside to dayside and Swarm B from dayside to nightside with ~ 2 hr local time separation of the orbital planes.

In Figures 4b&4c, the FACs observed before the negative pressure pulse were generally stronger than those after at Swarm, in agreement with the AMPERE observations. The only exception is that the FAC signal was significantly enhanced to ~ 2000 nT in magnitude shortly after the negative pressure pulse at Swarm A (highlighted in yellow in Figure 4b) at ~ 7 LT (Figure 4a). The magnetic field perturbations were mainly in the $-x$ direction (anti-sunward), which is the signature of a pair of FACs flowing downward at higher and upward at lower latitudes, respectively. The enhanced FAC pair had the same polarity of the regular R1/R2 FACs in the dawn sector. The enhanced δB_x magnitude was mainly due to the much-enhanced dawnward FAC at higher latitudes since the gradient (i.e., time rate of change) of δB_x was significantly higher at the poleward edge. The FACs observed by Swarm B at nearly the same time (yellow-highlighted interval in Figure 4c) but at ~ 11 LT (Figure 4a) did not show the same feature, neither did the subsequent FACs in the pre-midnight sector. When Swarm A returned to the same region in next orbit about 90 min later (~ 1615 UT), the FACs have returned to the weakened state. These observations indicate the much-enhanced downward FAC is a localized (near dawn) and transient (duration < 90 min) phenomenon in response to the sudden decrease of the solar wind dynamic pressure. The AMPERE observations did not capture such a localized transient response.

We now examine the EEJ profiles. As Swarm B is much closer to the local noon at the dayside equator, the EEJ signal is expected to be much stronger at Swarm B than Swarm A. Before the negative pressure pulse, the EEJ profile is not well defined at Swarm A (1323 UT, Figure 4d), mostly likely due to a very weak EEJ in early morning. But closer to the local noon, Swarm B detected the typical eastward EEJ profile at 1252 UT (Figure 4e) and 1426 UT (Figure 4f). Then about 17 min after the negative pressure pulse, Swarm A observed a well-defined westward EEJ, or counter electrojet (Figure 4e). The observed counter electrojet appeared to be a transient phenomenon. The EEJ returned to nominal eastward direction in the next two profiles, 1601 UT at Swarm B (Figure 4i) and 1632 UT at Swarm A (Figure 4f). These observations are in agreement with the ground-based EEJ currents in Figure 2.

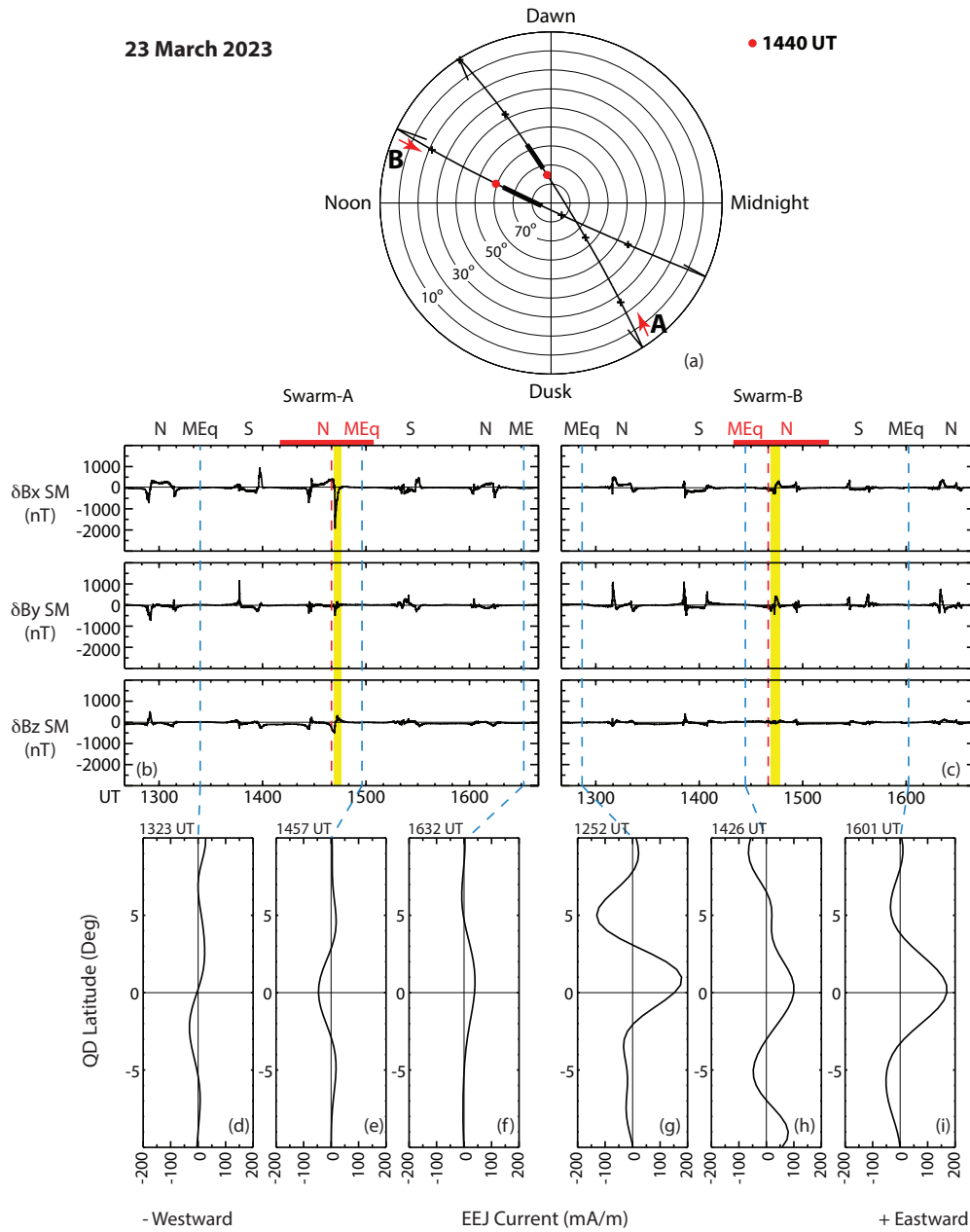


Figure 4. Swarm A and B observations of FACs and the EEJ: (a) Spacecraft trajectories near the negative pressure pulse; (b-c) the vector magnetic field residuals; (d-i) the latitudinal profiles of the EEJ around the magnetic equator.

3 Discussion

We first summarize the observations presented above.

- The solar wind dynamic pressure decreased suddenly and significantly at the boundary of the ICME that caused the 23 March 2023 magnetic storm. The negative pressure pulse arrived at the Earth at 1440 UT during the main phase of the storm and the IMF Bz fluctuated between northward and southward (Figure 1).
- The total large-scale FAC currents flowing into and out of the ionosphere decreased significantly soon after the arrival of the negative pressure pulse based (Figure 3). The overall geomagnetic activity level in the magnetosphere was weakened for more than 3 hrs, which paused the progression of the storm main phase. The activity level picked up again only after the IMF Bz turned strongly southward for an extended period during the passage of the ICME.
- Swarm A observed a significant enhancement of the downward FAC at the poleward edge of the FAC region near dawn shortly after the negative pressure pulse, which appeared to be localized and transient (Figure 4). Nearly simultaneous Swarm B observations closer to the local noon showed weakened FACs, consistent with the AMPERE observations.
- A transient counter electrojet was observed both in space by Swarm A (Figure 4) and on the ground (Figure 2) within minutes after the arrival of the negative pressure pulse. The counter electrojet lasted for ~ 1 hr and then returned to its regular eastward direction. The observed transient reversal of the EEJ to the westward direction suggests that the equatorial ionosphere experienced a brief period of a westward electric field after the negative pressure pulse.

These observations demonstrate the profound impact to the M-I system by the negative pressure pulse. The observed counter electrojet clearly shows that a transient westward electric field associated with the negative pressure pulse penetrated to the equatorial ionosphere from over-shielding (Hori et al., 2012; Fujita et al., 2012). The penetration electric field was much stronger in magnitude than the background eastward electric field from the wind dynamo so that the overall zonal electric field was reversed. Our observations indicated there was a sudden decrease of the dawn-to-dusk (eastward) convection electric field as evident by the sudden decrease of the total

FAC currents flowing into and out of the polar ionosphere immediately after the negative pressure pulse (Figure 3). The total FACs then gradually decrease with a time scale of hours. However, SYM-H, the ring current index, was flattened out in the same period, indicating the ring current did not immediately respond to the weakened convection electric field (Figure 1). The delayed response of the ring current reflects the time scale for the M-I system to gradually adjust to the expanded state of the magnetosphere with decreased level of plasma convection (Earle and Kelley, 1987). Thus, there was a short period when the low-latitude ionosphere was over-shielded and experienced a dusk-to-dawn (westward) electric field. Based on the duration of the counter-electrojet in the ground-based observations (Figure 2), the response of the ring current-R2 FAC system was delayed for ~6 min, and it took ~ 1 hr for the M-I system to gradually adjust itself to the decreased plasma convection level and the low-latitude ionosphere to return to be fully shielded.

To understand the transient responses and localized enhancement of FACs, it is necessary to review the current understanding of the underlying physical process. The M-I system responds to a sudden pressure pulse in two phases, including a preliminary impulse (PI) and a two-stage main impulse (MI) (e.g., Tamao, 1964a&b; Araki, 1977; Araki and Allen, 1982). The PI is due to the propagation and conversion of a compressional wave front launched from the magnetopause when the magnetosphere is suddenly compressed or expanded. The PI is transient by nature because its driver is the interaction between the pressure pulse and the magnetopause, which disappears in minutes after the impulse front propagates away from the dayside.

Although more previous studies focused on sudden pressure increases than decreases, the basic physics is the same. Based on Tamao's (1964a&b) pioneer work, Araki (1994) proposed a M-I coupling PI model to explain the global observations after geomagnetic sudden commencements. As illustrated in their Figure 12, the magnetopause moves inward and the dawn-to-dusk magnetopause current increases when the solar wind dynamic pressure suddenly increases. A compressional MHD wave is excited on the magnetopause, which propagates into the equatorial magnetosphere. The solar wind-magnetosphere interaction as a dynamo generates an enhanced dusk-to-dawn electric field at the magnetopause ($\mathbf{J} \cdot \mathbf{E} < 0$). A dusk-to-dawn electric field and associated inertia electric current are induced inside the magnetosphere. The extra magnetopause current and the inertia current would form a counterclockwise current loop. The compressional

wave will be converted into the transverse Alfvén wave due to the nonuniformity of the magnetosphere (Tamao, 1964b; Southwood and Kivelson, 1990). When the compressional wave front reaches the region where the Alfvén speed has a largest spatial gradient, converted Alfvén waves are generated and propagate along the field lines with associated FACs. A pair of FACs will be a part of the current loop, downward in the dusk side and upward in the dawn side. This process happens in time scale of minutes. So, the pair of FACs exists transiently at lower latitudes than the regular R1 currents with opposite polarity. A quantitative detail of the PI process is provided in the MHD simulations by Fujita et al. (2003a&b, 2005), and the source region of the MHD wave mode conversion for the generation of the transient FACs was found to be in the region of $6 < L < 7$ (Fujita et al., 2003a).

In the case of negative pressure pulses, the observations by Araki (1988) and simulations by Fujita et al. (2004, 2012) showed that the magnetospheric and ionospheric signatures mostly mirror those in pressure pulses. The negative pressure pulse causes the expansion of the magnetosphere and a decrease of the magnetopause current. The PI is associated with a dawn-to-dusk transient dynamo electric field at the magnetopause and induced electric field in the magnetosphere. The equatorial current loop would be clockwise to effectively reduce the magnetic field strength in the magnetosphere, and the pair of transient FACs would be downward in the dawnside and upward in the duskside, in the same polarity of the regular R1 currents. The transient and localized enhancement of the downward FAC observed by Swarm A near dawn (Figure 4) matches the predicted polarity of the FACs. However, our observations differ in an important aspect from the model prediction. The transient, localized FAC enhancement was observed at the poleward edge of the FAC region, implying the source region was near the magnetopause, as in the earliest work of Tamao (1964a). Further theoretical and numerical investigation is still needed to understand the source region of the transient FACs during the PI. In addition, understanding the role of the ring current/R2 FAC system to the undershielding/overshielding and its restoration is particularly needed in future simulations.

4 Conclusions

A drastic decrease of the solar wind dynamic pressure occurred during main phase of the 23 March 2023 geomagnetic storm in association with the boundary between the ICME and its sheath. Our observations show that the negative pressure pulse had significant impact to the M-I system. It weakened the overall geomagnetic activities and plasma convection and paused the progression of the storm main phase for ~ 3 hrs. Due to the sudden decrease of the dawn-to-dusk convection electric field, there was a transient period when the low-latitude ionosphere was over-shielded and experienced a brief period of dusk-to-dawn (westward) penetration electric field. The transient westward penetration electric field reversed the direction of the equatorial electrojet, and the counter electrojet was observed both in space and on the ground. The response of the ring current-R2 FAC system was delayed for ~ 6 min, and it took ~ 1 hr for the M-I system to adjust itself to the decreased plasma convection level until the low-latitude ionosphere was fully shielded again. Although the overall large-scale FACs were weakened by the negative pressure pulse, a transient, localized enhancement of downward FAC was observed near dawn, consistent with the mechanism for transmitting MHD disturbances in the M-I coupling after the negative pressure pulse. But the latitudinal location of the localized FAC enhancement differed from the model prediction, which calls further investigation of the MI coupling in response to the pressure pulse.

Acknowledgements

GL thanks Lan Jian for helpful discussion. EY was partially supported by the AFOSR (FA9550-20-1-0119) and NSF (AGS-1848730) grants. NB was partially supported by NASA Internal Scientist Funding Model on Mesoscale Dynamics.

Data Availability Statement

The OMNI data are available at <https://omniweb.gsfc.nasa.gov>. The JICA and PIUR magnetometer data are available at <https://zenodo.org/records/10823058>. The KOU and TTB magnetometer data are available at INTERMAGNET (www.intermagnet.org). The AMPERE data are available at <https://ampere.jhuapl.edu>. The Swarm data are accessible at <https://earth.esa.int/eogateway/missions/swarm/data>.

References

- Alken, P., S. Maus, A. Chulliat, P. Vigneron, O. Sirol, and G. Hulot (2015), Swarm equatorial electric field chain: First results, *Geophys. Res. Lett.*, 42, 673–680. <https://doi.org/10.1002/2014GL062658>
- Anderson, D., A. Anghel, J. Chau, and O. Veliz (2004), Daytime vertical $E \times B$ drift velocities inferred from ground-based magnetometer observations at low latitudes, *Space Weather*, 2, S11001. <https://doi.org/10.1029/2004SW000095>
- Araki, T. (1977), Global structure of geomagnetic sudden commencements, *Planet. Space Sci.*, 25, 373. [https://doi.org/10.1016/0032-0633\(77\)90053-8](https://doi.org/10.1016/0032-0633(77)90053-8)
- Araki, T. (1994). A physical model of the geomagnetic sudden commencement. *Geophysical Monograph-American Geophysical Union*, 81, 183-183. <https://doi.org/10.1029/GM081p0183>
- T. Araki, J. H. Allen (1982), Latitudinal reversal of polarization of the geomagnetic sudden commencement, *J. Geophys. Res.*, 87, 5207– 5216. <https://doi.org/10.1029/JA087iA07p05207>
- Araki, T. and H. Nagano (1988), Geomagnetic response to sudden expansions of the magnetosphere, *J. Geophys. Res.*, 93, 3983–3988. <https://doi.org/10.1029/JA093iA05p03983>
- Earle, G. D., and M. C. Kelley (1987), Spectral studies of the sources of ionospheric electric fields, *J. Geophys. Res.*, 92(A1), 213–224. <https://doi.org/10.1029/JA092iA01p00213>
- Fejer, B., C. Gonzales, D. Farley, M. Kelley, and R. Woodman (1979), Equatorial electric fields during magnetically disturbed conditions 1. The effect of the interplanetary magnetic field, *J. Geophys. Res.*, 84(A10), 5797–5802. <https://doi.org/10.1029/JA084iA10p05797>

Fejer BG, Laranja SR and Condor P (2024), Multi-process driven unusually large equatorial
 perturbation electric fields during the April 2023 geomagnetic storm. *Front. Astron. Space Sci.*
 11:1351735. <https://doi.org/10.3389/fspas.2024.1351735>

Fujita, S., T. Tanaka, T. Kikuchi, K. Fujimoto, K. Hosokawa, and M. Itonaga (2003a), A numerical
 simulation of the geomagnetic sudden commencement: 1. Generation of the field-aligned current
 associated with the preliminary impulse, *J. Geophys. Res.*, 108(A12), 1416.
<https://doi.org/10.1029/2002JA009407>

Fujita, S., T. Tanaka, T. Kikuchi, K. Fujimoto, and M. Itonaga (2003b), A numerical simulation of
 the geomagnetic sudden commencement: 2. Plasma processes in the main impulse, *J. Geophys.*
Res., 108(A12), 1417. <https://doi.org/10.1029/2002JA009763>

Fujita, S., T. Tanaka, T. Kikuchi, and S. Tsunomura (2004), A numerical simulation of a negative
 sudden impulse, *Earth Planets Space*, 56, 463–472. <https://doi.org/10.1186/BF03352499>

Fujita, S., T. Tanaka, and T. Motoba (2005), A numerical simulation of the geomagnetic sudden
 commencement: 3. A sudden commencement in the magnetosphere-ionosphere compound system,
J. Geophys. Res., 110, A11203. <https://doi.org/10.1029/2005JA011055>

Fujita, S., H. Yamagishi, K. T. Murata, M. Den, and T. Tanaka (2012), A numerical simulation of a
 negative solar wind impulse: Revisited, *J. Geophys. Res.*, 117, A09219.
<https://doi.org/10.1029/2012JA017526>

Heelis, R. A. (2004). Electrodynamics in the low and middle latitude ionosphere: A tutorial. *Journal*
of Atmospheric and Solar-Terrestrial Physics, 66(10), 825-
 838. <https://doi.org/10.1016/j.jastp.2004.01.034>

Hori, T., A. Shinbori, N. Nishitani, T. Kikuchi, S. Fujita, T. Nagatsuma, O. Troshichev, K. Yumoto,
 A. Moiseyev, and K. Seki (2012), Evolution of negative SI-induced ionospheric flows observed by

SuperDARN King Salmon HF radar, J. Geophys. Res., 117, A12223,
<https://doi.org/10.1029/2012JA018093>

Jaggi, R. K., and R. A. Wolf (1973), Self-consistent calculation of the motion of a sheet of ions in the magnetosphere, J. Geophys. Res.; Space Physics, 78(16), 2852-2866.
<https://doi.org/10.1029/JA078i016p02852>

Kelley, M. C., J. J. Makela, J. L. Chau, and M. J. Nicolls (2003), Penetration of the solar wind electric field into the magnetosphere/ionosphere system, Geophys. Res. Lett., 30, 1158.
<https://doi.org/10.1029/2002GL016321>

Morschhauser, A., Brando Soares, G., Haseloff, J., Bronkalla, O., Protásio, J., Pinheiro, K., and Matzka, J. (2017): The magnetic observatory on Tatuoca, Belém, Brazil: history and recent developments, Geosci. Instrum. Method. Data Syst., 6, 367–376. <https://doi.org/10.5194/gi-6-367-2017>

Nishida, A. (1968), Coherence of geomagnetic $DP\ 2$ fluctuations with interplanetary magnetic variations, J. Geophys. Res.: Space Physics, 73, 5549-5559.
<https://doi.org/10.1029/JA073i017p05549>

Richmond, A. D. (1973). Equatorial electrojet-1. Development of a model including winds and instabilities. *Journal of Atmospheric and Terrestrial Physics*, **35**(6), 1083-1103. [https://doi.org/10.1016/0021-9169\(73\)90007-x](https://doi.org/10.1016/0021-9169(73)90007-x)

Southwood, D. J. (1977), The role of hot plasma in magnetospheric convection, J. Geophys. Res., 82(35), 5512–5520. <https://doi.org/10.1029/JA082i035p05512>

Southwood, D. J., and M. G. Kivelson (1990), The magnetohydrodynamic response of the magnetospheric cavity to changes in solar wind pressure, J. Geophys. Res., 95, 2301–2309.
<https://doi.org/10.1029/JA095iA03p02301>

479 Tamao, T. (1964a), The structure of three-dimensional hydromagnetic waves in a uniform cold
 480 plasma, J. Geomagn. Geoelectr., 16, 89– 114, 1964a. <https://doi.org/10.5636/jgg.16.89>
 481
 482 Tamao, T. (1964b), A hydromagnetic interpretation of geomagnetic SSC*, Rep. Ionos. Space Res.
 483 Jpn., 18, 16– 31.
 484
 485 Yizengaw, E., M. B. Moldwin, A. Mebrahtu, B. Damtie, E. Zesta, C. E. Valladares, and P. Doherty
 486 (2011), Comparison of storm time equatorial ionospheric electrodynamics in the African and
 487 American sectors, Journal of Atmospheric and Solar-Terrestrial Physics, 73, 156-163.
 488 <https://doi.org/10.1016/j.jastp.2010.08.008>
 489
 490 Yizengaw, E., M. B. Moldwin, E. Zesta, C. M. Biouele, B. Damtie, A. Mebrahtu, B. Rabiou, C. F.
 491 Valladares, and R. Stoneback (2014), The longitudinal variability of equatorial electrojet and
 492 vertical drift velocity in the African and American sector, Ann. Geophys., 32, 231–238.
 493 <https://doi.org/10.5194/angeo-32-231-2014>
 494
 495 Yizengaw, E., Moldwin, M. B., Zesta, E., Magoun, M., Pradipta, R., Biouele, C. M., et al. (2016).
 496 Response of the equatorial ionosphere to the geomagnetic DP 2 current system. Geophysical
 497 Research Letters, 43(14), 7364–7372. <https://doi.org/10.1002/2016gl070090>

**Solar wind-magnetosphere-ionosphere coupling and its impact on equatorial
ionospheric electrodynamics during the 23 March 2023 geomagnetic storm:
Effect of sudden decrease of solar wind dynamic pressure**

Guan Le¹, Guiping Liu¹, and Endawoke Yizengaw², Chin-Chun Wu³, Yihua Zheng¹, Sarah Vines^{4,5},
Natalia Buzulukova^{1,6}

¹NASA Goddard Space Flight Center, Greenbelt, MD (guan.le@nasa.gov)

²The Aerospace Corporation, El Segundo, CA

³Naval Research Laboratory, Washington, DC

⁴Applied Physics Laboratory, Laurel, MD

⁵Now at Southwest Research Institute, San Antonio, TX

⁶University of Maryland, College Park, MD

Corresponding author: Guan Le (guan.le@nasa.gov)

Key Points:

1. Direct evidence of prompt penetration of electric field in the equatorial ionosphere caused by negative solar wind pressure pulse
2. Transient counter electrojet caused by westward penetration electric field after the arrival of negative pressure pulse
3. Significant decrease of global large-scale FACs and transient enhancement of localized FAC in response to negative pressure pulse

Abstract

We present a study of the magnetosphere-ionosphere coupling during the 23 March 2023 magnetic storm, focusing on the effect of the drastic decrease of the solar wind dynamic pressure occurred during the main phase. Our observations show that the negative pressure pulse had significant impact to the magnetosphere-ionosphere system. It weakened large-scale field-aligned currents and paused the progression of the storm main phase for ~ 3 hrs. Due to the sudden decrease of the plasma convection after the negative pressure pulse, the low-latitude ionosphere was over-shielded and experienced a brief period of westward penetration electric field, which reversed the direction of the equatorial electrojet. The counter electrojet was observed both in space and on the ground. A transient, localized enhancement of downward field-aligned current was observed near dawn, consistent with the mechanism for transmitting MHD disturbances from magnetosphere to the ionosphere after the negative pressure pulse.

Plain Language Summary

The solar wind is a continuous stream of charged particles blowing from the Sun. The Earth's magnetic field forms a protective shield around our planet, called the magnetosphere, which deflects most of the solar wind particles away from the Earth. Disturbances in the solar wind can interact with the magnetosphere and impact the Earth's upper atmosphere (ionosphere). The interaction creates electric fields forcing charged particles to move in the magnetosphere, which creates electric currents flowing along the magnetic field lines connecting to the high-latitude ionosphere and drives the movement of charged particles there. The low-latitude ionosphere is generally shielded from these electric fields. Sudden changes in the solar wind can break such balance, leading to the electric field penetration to low latitudes. We examined how the magnetosphere and ionosphere interacted during the 23 March 2023 geomagnetic storm, focusing on what happened when the solar wind dynamic pressure suddenly decreased. We found the pressure drop caused a sudden decrease of the high-latitude electric field, resulting in a brief period of overshielding and the electric field in the equatorial ionosphere reversed its direction. This changed the direction of the equatorial electrojet, a major electric current in the ionosphere at the magnetic equator.

1 Introduction

In steady-state conditions, the low-latitude ionosphere is shielded from the high-latitude convection electric field due to the partial ring current-associated region-2 (R2) field-aligned currents (FACs) which act to oppose the electric field associated with region-1 (R1) FACs (e.g., Southwood, 1977). However, it can be directly coupled to the magnetospheric disturbances through prompt penetration of the convection electric field during active times (Nishida, 1968; Jaggi and Wolf, 1973; Fejer et al., 1979).

The equatorial electrojet (EEJ), an intense band of eastward electric current flowing along the dayside magnetic equator in the E-region ionosphere (~ 110 km altitude), is driven by an eastward zonal electric field from plasma-neutral collisional interactions known as the E-region wind dynamo (Richmond, 1973; Heelis, 2004). The intensity and polarity of the EEJ respond directly to the perturbations of the zonal electric field. Variations of the EEJ often serve as an indicator for the equatorial zonal electric field perturbations, which can be caused by either neutral wind changes from lower atmosphere forcing or prompt penetration electric fields (PPEFs) from enhanced magnetosphere-ionosphere (M-I) coupling. Many studies have used EEJ variations to probe the presence of PPEFs that are attributed to interplanetary magnetic field (IMF) variations (e.g., Yizengaw et al., 2011, 2016) or solar wind dynamic pressure pulses (e.g., Nilam et al., 2020, 2023). Understanding the sources and the process of PPEFs continues to be a subject of ongoing investigation (Kelly et al., 2003; Fejer et al., 2024).

This paper reports the observations of the M-I coupling and its effect on the equatorial ionosphere in response to a sudden decrease of the solar wind dynamic pressure during the main phase of the 23 March 2023 geomagnetic storm. Figure 1 shows 1-min resolution OMNI data for the IMF and solar wind parameters along with ground-based SYM-H index for 23-25 March 2023. This large storm (minimum Dst ~ -170 nT, Kp ~ 7) was associated with the passage of an interplanetary coronal mass ejection (ICME), triggered by the southward IMF in both the sheath and the ICME regions. A drastic density decrease was observed at the boundary crossing from the sheath to the ICME by the WIND spacecraft. As a result, a significant negative solar wind pressure pulse hit the

Earth's magnetosphere during the main phase of the storm (1440 UT, marked by the red dashed line in Figure 1). The solar wind density as well as the dynamic pressure decreased by a factor of ~ 10 .

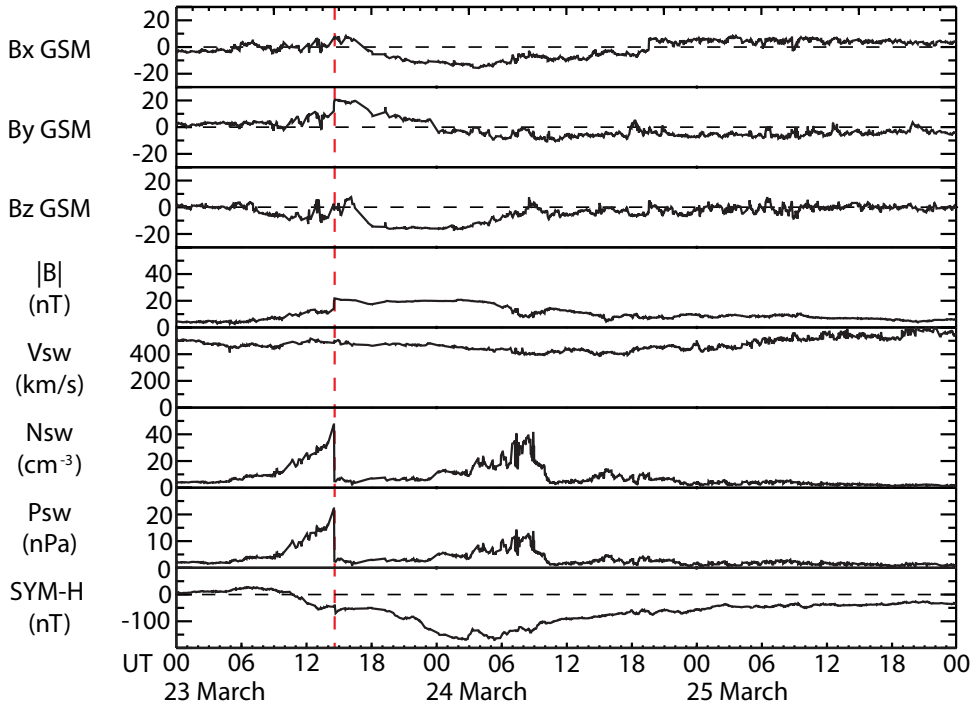


Figure 1. The 1-min resolution OMNI data with IMF/solar wind parameters (top 7 panels) and SYM-H index (bottom panel) for 23 March 2023 magnetic storm. The negative pressure pulse during the main phase of the storm is marked by the red dashed line.

We examine how FACs at high latitudes and the EEJ at the equator responded to the negative pressure pulse using both space and ground-based magnetic field data. In the following sections, we first present evidence for a transient PPEF associated with the pressure pulse from the ground based EEJ observations. Then we examine the response of large-scale FACs globally by AMPERE and locally by Swarm satellites. We also analyze the EEJ observations in space by Swarm, which provide additional evidence for the transient PPEF associated with the pressure pulse. Finally, we discuss the dynamic processes involving solar wind pressure pulse interacting with the magnetosphere and coupling into the polar ionosphere, that allow us to understand the behaviors of the equatorial ionosphere.

2 Observations

2.1 Ground-based Observations of the EEJ

The EEJ signals can be obtained from a pair of ground magnetometer stations located near the magnetic equator on the same meridian, one directly under the EEJ at the equator (within $\pm 3.5^\circ$) and the other just off the EEJ region (6° – 9° from the magnetic equator) (Anderson et al., 2004; Yizengaw et al., 2014). The EEJ signals can only be detected by the station at the magnetic equator because the EEJ current is confined in a narrow latitudinal band (within $\pm 3^\circ$). But both stations are expected to record the same magnetic field variations from other large-scale current sources, such as the solar quiet (Sq) currents, the ring current, and the magnetopause current. The EEJ signals are extracted from the difference of the H-components between the two stations. In this study, we used two pairs of geomagnetic observatories at two meridians ($\sim 80^\circ\text{W}$ and $\sim 50^\circ\text{W}$). One pair is located at Jicamarca (JICA, $11.95^\circ\text{S}/76.87^\circ\text{W}$ GEO, $\text{MLat} = 0.6^\circ\text{N}$) and Piura (PIUR, $5.2^\circ\text{S}/80.6^\circ\text{W}$ GEO, $\text{MLat} = 6.9^\circ\text{N}$) in Peru. The other pair is located at Tatuoca, Brazil (TTB, $1.21^\circ\text{S}/48.5^\circ\text{W}$ GEO) and Kourou, French Guyana (KOU, $5.21^\circ\text{N}/52.7^\circ\text{W}$ GEO). TTB and KOU are well located under and far enough from the EEJ, respectively. They are within the region of South Atlantic Anomaly with rapid northward moving of the magnetic equator, and the magnetic equator passed the TTB in March 2013 (Morschhauser et al., 2017).

Figure 2 shows the magnetic field observations from the 2 pairs of ground observatories on 23 March 2023 with three subpanels for each pair, from top to bottom, showing the H-component with the background removed (δH) off the magnetic equator, at the magnetic equator, and the EEJ signal (δH_{EEJ} , the differences between δH at the geomagnetic equator and off the equator), respectively. The horizontal bar in the 3rd subpanel indicates dayside hours (6–18 LT) at the equator station. The red dashed line indicates the time of the negative pressure pulse (1440 UT) in Figure 1. The local time (LT) of the pressure pulses at the two equator stations are also noted in Figure 2.

The eastward zonal electric field from the wind dynamo drives the eastward EEJ, producing a positive magnetic field perturbation ($\delta H_{EEJ} > 0$) in the dayside. This is generally the case in Figure 2 except for a brief period immediately following the negative pressure pulse. There was a transient negative impulse of the H-component at all the stations, consisting of a sharp decrease (~ 6 min) and

a relatively gradual (~ 1 hour) return, apparently due to the sudden decrease of the magnetopause current and expansion of the magnetosphere in response to the negative pressure pulse (Araki and Nagano, 1988). However, the transient negative impulse at the equator station is much stronger than its off-equator counterpart, and the EEJ signature reversed its sign showing a transient counter electrojet flowing westward. This observation indicates the negative pressure pulse set up a transient westward electric field (~ 1 hour) in the equatorial ionosphere.

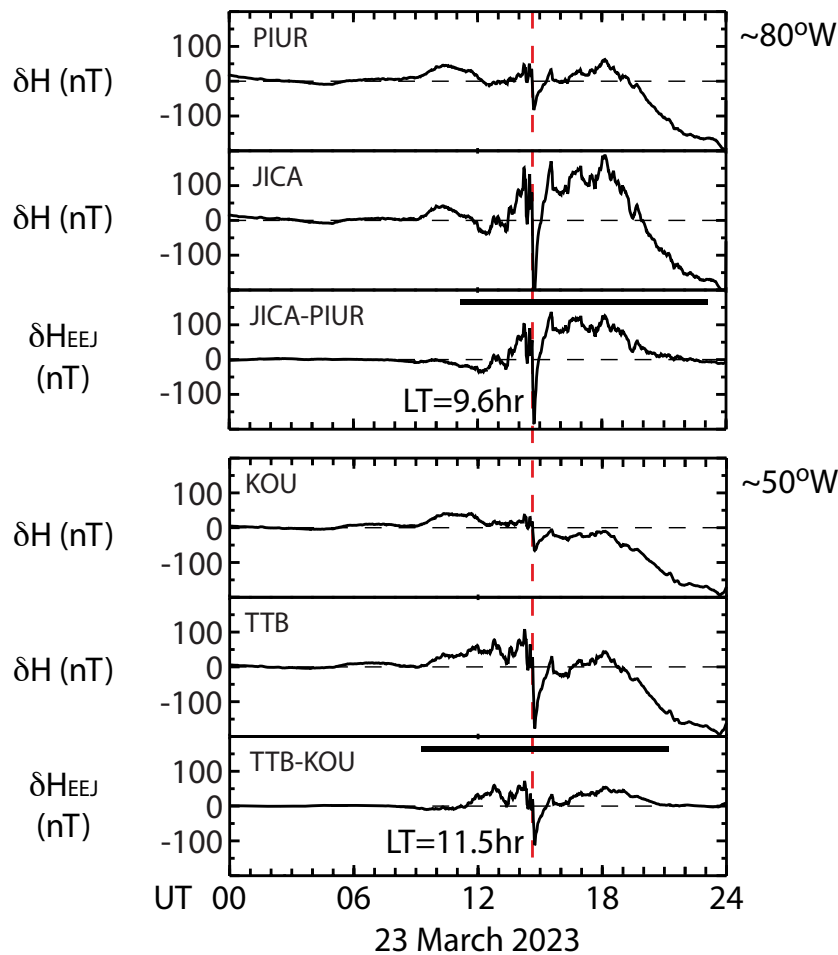


Figure 2. Ground-based observations of the H-component from 2 pairs of ground observatories on 23 March 2023, JICA-PIUR and TTB-KOU, respectively. The red dashed line marks the negative pressure pulse in Figure 1. The black horizontal bars indicate the daytime (06-16 LT) at the equator stations.

2.2 AMPERE Observations of Large-scale FACs

AMPERE observations of large-scale FACs are derived from global measurements of magnetic field perturbations from the Iridium constellation of more than 70 near-polar orbiting satellites [Anderson et al., 2000]. It collects 10-min data to generate one global pattern of large-scale FAC distributions and provides a continuous monitor of the state of the global M-I system. (AMPERE data will unlikely reveal transient and localized variations due to the limitation of spatial and temporal resolution.) Figure 3 shows the AMPERE observations of the total field-aligned currents flowing into and out of the ionosphere on 23 March 2023 (Figure S1 provides the magnetic field perturbations and global FAC maps). The total upward current out of one hemisphere is calculated by integrating all the upward current density over the entire area above 40° latitude, and likewise for the total downward current. Again, the red dashed vertical line corresponds to the negative pressure pulse in Figure 1.

Starting from ~ 07 UT, the total FACs gradually intensified as the storm progressed with the SYM-H index became more negative, representing an increasing active magnetosphere as FACs facilitate the electromagnetic energy input from the magnetosphere into the ionosphere. There is a brief period (~ 1 hr) of total current drop starting at ~13 UT, apparently associated with the northward excursion of the IMF Bz component (Figure 1) which turned off the dayside reconnection and reduced the magnetospheric convection temporally.

Figure 3 shows the total currents responded to the negative pressure in two stages. The total currents dropped sharply at ~1440 UT due to the sudden sunward motion of the magnetopause and expansion of the magnetosphere. The sudden reduction of the magnetopause current also caused a step decrease of the SYM-H index (Figure 1). Then the total currents continued to decrease gradually. The decreasing trend of the SYM-H index has flattened out within the storm main phase, indicating the pause of the ring current development (Figure 1). This is expected as IMF Bz fluctuated around zero and the expanded magnetosphere adjusted to the new state of reduced geomagnetic activity level. At ~1630 UT, the IMF Bz gradually turned southward, which terminated the decreasing trend of the total currents. At ~ 18 UT, both the total currents (Figure 3) and the SYM-H index (Figure 1) showed that the magnetospheric activities began to intensify

rapidly with the prolonged steady southward IMF in the ICME. In summary of the AMPERE observations, large-scale FACs were significantly weakened by the negative pressure pulse.

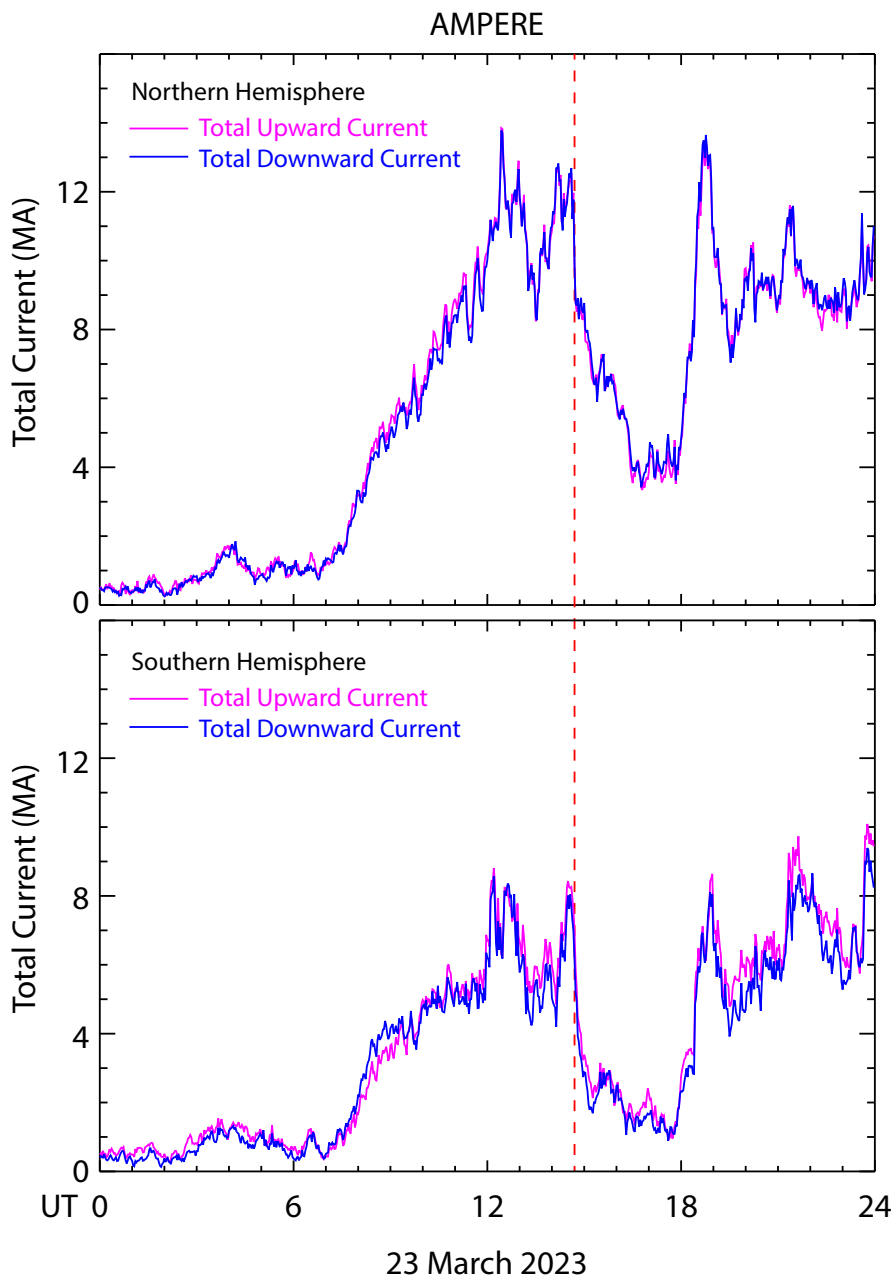


Figure 3. AMPERE Observations of the total amount of upward and downward FACs in northern and southern hemisphere, respectively.

2.3 Swarm Observations of FACs and EEJ

Swarm is a three-satellite mission in a high-inclination (87.5°) low-Earth orbit, which provides vector magnetic field data for frequent in situ measurements of FACs at high latitudes (Lühr et al., 2015) and scale magnetic field strength for the EEJ in the equatorial region (Alken et al., 2015). Among the three satellites, A and C form a pair flying side by side at the same altitude (~ 460 km) with a longitudinal separation of 1.4° . Swarm B has slightly higher altitude (~ 530 km) and its orbital plane slowly drifts apart from those of Swarm A/C. In this study, we used two official Swarm level-2 data products: (1) the vector magnetic field residuals $\delta \mathbf{B}$ for the study of FACs, and (2) the height-integrated latitudinal profile of eastward EEJ current. The EEJ current profile is estimated from the Swarm scalar magnetic field measurements by isolating the EEJ signal from the many other geomagnetic sources and then fitting the EEJ signal with a line current model (Alken et al., 2015). The EEJ current peak at the magnetic equator provides a good estimate of the EEJ strength.

Figure 4 presents an overview of the Swarm observations. Figure 4a shows the spacecraft orbits for the polar cap pass near 1440 UT, the intervals marked by the red bars in Figures 4b/4c. Figures 4b and 4c contain 4 hours of Swarm vector magnetic field residuals $\delta \mathbf{B}$ in solar magnetic (SM) coordinate system centered at 1440 UT (red dashed line) for Swarm A and B, respectively. Swarm C data are nearly the same as Swarm A (not shown). During this interval, Swarm made 5 passes of the polar cap, denoted by N (S) for the northern (southern) hemisphere, and 3 crossings of the dayside magnetic equator marked by MEq and the blue dashed lines. The perturbations in $\delta \mathbf{B}$ are the signals of FACs, occurring at auroral latitudes on both sides of the magnetic pole. The latitudinal profiles of the estimated EEJ current at the dayside magnetic equator crossings are presented in Figures 4d-4f for Swarm A and 4g-4i for Swarm B. The positive current is for eastward EEJ.

Both Swarm A and B were in the dayside morning sector over the northern polar cap at the time of the negative pressure pulse (red dots in Figure 4a). In Figure 4a, the tick marks on each trajectory are separated by 10 min. The red arrows indicate the directions of the spacecraft motion. Swarm A was moving from nightside to dayside and Swarm B from dayside to nightside with ~ 2 hr local time separation of the orbital planes.

In Figures 4b&4c, the FACs observed before the negative pressure pulse were generally stronger than those after at Swarm, in agreement with the AMPERE observations. The only exception is that the FAC signal was significantly enhanced to ~ 2000 nT in magnitude shortly after the negative pressure pulse at Swarm A (highlighted in yellow in Figure 4b) at ~ 7 LT (Figure 4a). The magnetic field perturbations were mainly in the $-x$ direction (anti-sunward), which is the signature of a pair of FACs flowing downward at higher and upward at lower latitudes, respectively. The enhanced FAC pair had the same polarity of the regular R1/R2 FACs in the dawn sector. The enhanced δB_x magnitude was mainly due to the much-enhanced dawnward FAC at higher latitudes since the gradient (i.e., time rate of change) of δB_x was significantly higher at the poleward edge. The FACs observed by Swarm B at nearly the same time (yellow-highlighted interval in Figure 4c) but at ~ 11 LT (Figure 4a) did not show the same feature, neither did the subsequent FACs in the pre-midnight sector. When Swarm A returned to the same region in next orbit about 90 min later (~ 1615 UT), the FACs have returned to the weakened state. These observations indicate the much-enhanced downward FAC is a localized (near dawn) and transient (duration < 90 min) phenomenon in response to the sudden decrease of the solar wind dynamic pressure. The AMPERE observations did not capture such a localized transient response.

We now examine the EEJ profiles. As Swarm B is much closer to the local noon at the dayside equator, the EEJ signal is expected to be much stronger at Swarm B than Swarm A. Before the negative pressure pulse, the EEJ profile is not well defined at Swarm A (1323 UT, Figure 4d), mostly likely due to a very weak EEJ in early morning. But closer to the local noon, Swarm B detected the typical eastward EEJ profile at 1252 UT (Figure 4e) and 1426 UT (Figure 4f). Then about 17 min after the negative pressure pulse, Swarm A observed a well-defined westward EEJ, or counter electrojet (Figure 4e). The observed counter electrojet appeared to be a transient phenomenon. The EEJ returned to nominal eastward direction in the next two profiles, 1601 UT at Swarm B (Figure 4i) and 1632 UT at Swarm A (Figure 4f). These observations are in agreement with the ground-based EEJ currents in Figure 2.

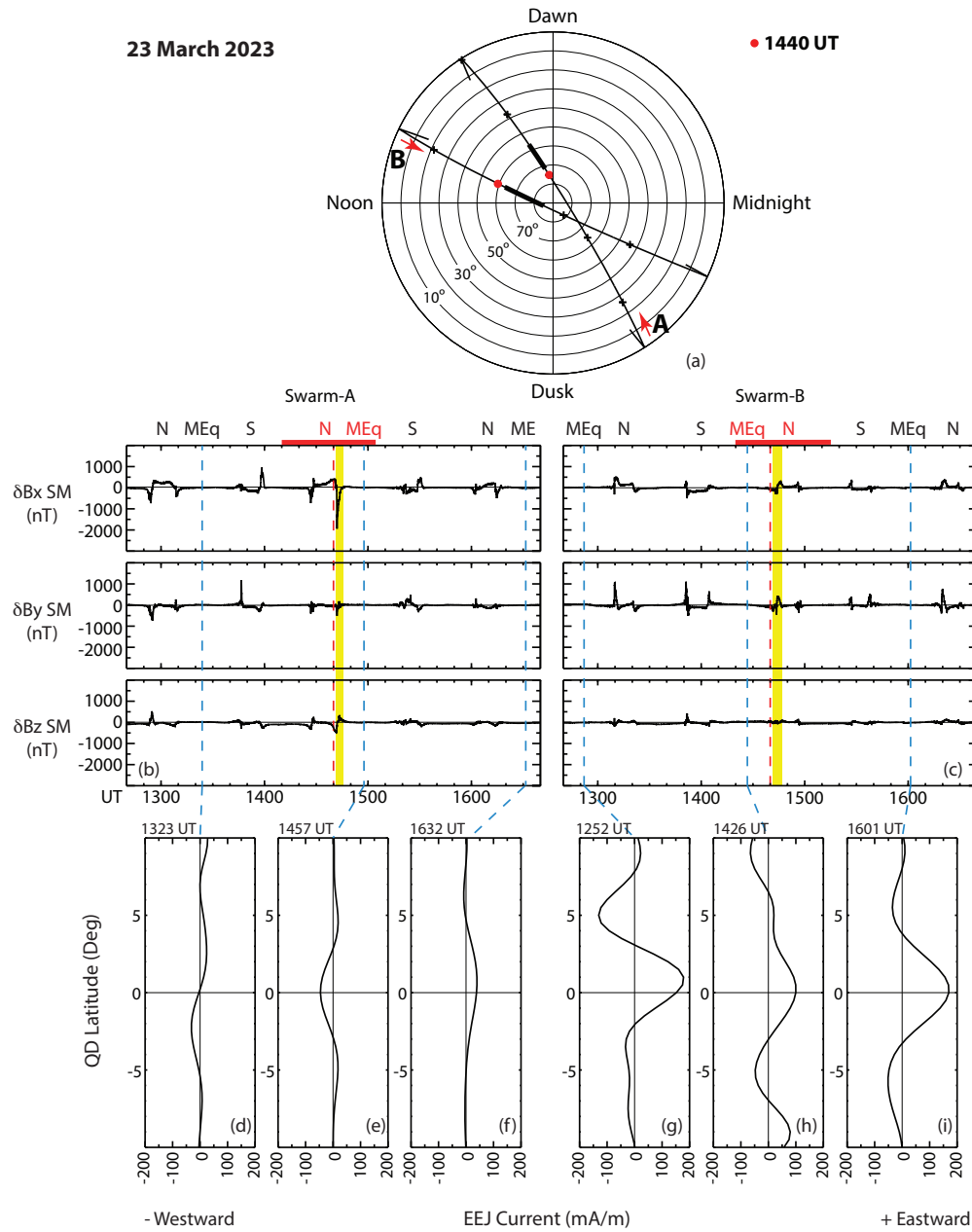


Figure 4. Swarm A and B observations of FACs and the EEJ: (a) Spacecraft trajectories near the negative pressure pulse; (b-c) the vector magnetic field residuals; (d-i) the latitudinal profiles of the EEJ around the magnetic equator.

3 Discussion

We first summarize the observations presented above.

- The solar wind dynamic pressure decreased suddenly and significantly at the boundary of the ICME that caused the 23 March 2023 magnetic storm. The negative pressure pulse arrived at the Earth at 1440 UT during the main phase of the storm and the IMF Bz fluctuated between northward and southward (Figure 1).
- The total large-scale FAC currents flowing into and out of the ionosphere decreased significantly soon after the arrival of the negative pressure pulse based (Figure 3). The overall geomagnetic activity level in the magnetosphere was weakened for more than 3 hrs, which paused the progression of the storm main phase. The activity level picked up again only after the IMF Bz turned strongly southward for an extended period during the passage of the ICME.
- Swarm A observed a significant enhancement of the downward FAC at the poleward edge of the FAC region near dawn shortly after the negative pressure pulse, which appeared to be localized and transient (Figure 4). Nearly simultaneous Swarm B observations closer to the local noon showed weakened FACs, consistent with the AMPERE observations.
- A transient counter electrojet was observed both in space by Swarm A (Figure 4) and on the ground (Figure 2) within minutes after the arrival of the negative pressure pulse. The counter electrojet lasted for ~ 1 hr and then returned to its regular eastward direction. The observed transient reversal of the EEJ to the westward direction suggests that the equatorial ionosphere experienced a brief period of a westward electric field after the negative pressure pulse.

These observations demonstrate the profound impact to the M-I system by the negative pressure pulse. The observed counter electrojet clearly shows that a transient westward electric field associated with the negative pressure pulse penetrated to the equatorial ionosphere from over-shielding (Hori et al., 2012; Fujita et al., 2012). The penetration electric field was much stronger in magnitude than the background eastward electric field from the wind dynamo so that the overall zonal electric field was reversed. Our observations indicated there was a sudden decrease of the dawn-to-dusk (eastward) convection electric field as evident by the sudden decrease of the total

FAC currents flowing into and out of the polar ionosphere immediately after the negative pressure pulse (Figure 3). The total FACs then gradually decrease with a time scale of hours. However, SYM-H, the ring current index, was flattened out in the same period, indicating the ring current did not immediately respond to the weakened convection electric field (Figure 1). The delayed response of the ring current reflects the time scale for the M-I system to gradually adjust to the expanded state of the magnetosphere with decreased level of plasma convection (Earle and Kelley, 1987). Thus, there was a short period when the low-latitude ionosphere was over-shielded and experienced a dusk-to-dawn (westward) electric field. Based on the duration of the counter-electrojet in the ground-based observations (Figure 2), the response of the ring current-R2 FAC system was delayed for ~ 6 min, and it took ~ 1 hr for the M-I system to gradually adjust itself to the decreased plasma convection level and the low-latitude ionosphere to return to be fully shielded.

To understand the transient responses and localized enhancement of FACs, it is necessary to review the current understanding of the underlying physical process. The M-I system responds to a sudden pressure pulse in two phases, including a preliminary impulse (PI) and a two-stage main impulse (MI) (e.g., Tamao, 1964a&b; Araki, 1977; Araki and Allen, 1982). The PI is due to the propagation and conversion of a compressional wave front launched from the magnetopause when the magnetosphere is suddenly compressed or expanded. The PI is transient by nature because its driver is the interaction between the pressure pulse and the magnetopause, which disappears in minutes after the impulse front propagates away from the dayside.

Although more previous studies focused on sudden pressure increases than decreases, the basic physics is the same. Based on Tamao's (1964a&b) pioneer work, Araki (1994) proposed a M-I coupling PI model to explain the global observations after geomagnetic sudden commencements. As illustrated in their Figure 12, the magnetopause moves inward and the dawn-to-dusk magnetopause current increases when the solar wind dynamic pressure suddenly increases. A compressional MHD wave is excited on the magnetopause, which propagates into the equatorial magnetosphere. The solar wind-magnetosphere interaction as a dynamo generates an enhanced dusk-to-dawn electric field at the magnetopause ($\mathbf{J} \cdot \mathbf{E} < 0$). A dusk-to-dawn electric field and associated inertia electric current are induced inside the magnetosphere. The extra magnetopause current and the inertia current would form a counterclockwise current loop. The compressional

wave will be converted into the transverse Alfvén wave due to the nonuniformity of the magnetosphere (Tamao, 1964b; Southwood and Kivelson, 1990). When the compressional wave front reaches the region where the Alfvén speed has a largest spatial gradient, converted Alfvén waves are generated and propagate along the field lines with associated FACs. A pair of FACs will be a part of the current loop, downward in the dusk side and upward in the dawn side. This process happens in time scale of minutes. So, the pair of FACs exists transiently at lower latitudes than the regular R1 currents with opposite polarity. A quantitative detail of the PI process is provided in the MHD simulations by Fujita et al. (2003a&b, 2005), and the source region of the MHD wave mode conversion for the generation of the transient FACs was found to be in the region of $6 < L < 7$ (Fujita et al., 2003a).

In the case of negative pressure pulses, the observations by Araki (1988) and simulations by Fujita et al. (2004, 2012) showed that the magnetospheric and ionospheric signatures mostly mirror those in pressure pulses. The negative pressure pulse causes the expansion of the magnetosphere and a decrease of the magnetopause current. The PI is associated with a dawn-to-dusk transient dynamo electric field at the magnetopause and induced electric field in the magnetosphere. The equatorial current loop would be clockwise to effectively reduce the magnetic field strength in the magnetosphere, and the pair of transient FACs would be downward in the dawnside and upward in the duskside, in the same polarity of the regular R1 currents. The transient and localized enhancement of the downward FAC observed by Swarm A near dawn (Figure 4) matches the predicted polarity of the FACs. However, our observations differ in an important aspect from the model prediction. The transient, localized FAC enhancement was observed at the poleward edge of the FAC region, implying the source region was near the magnetopause, as in the earliest work of Tamao (1964a). Further theoretical and numerical investigation is still needed to understand the source region of the transient FACs during the PI. In addition, understanding the role of the ring current/R2 FAC system to the undershielding/overshielding and its restoration is particularly needed in future simulations.

4 Conclusions

A drastic decrease of the solar wind dynamic pressure occurred during main phase of the 23 March 2023 geomagnetic storm in association with the boundary between the ICME and its sheath. Our observations show that the negative pressure pulse had significant impact to the M-I system. It weakened the overall geomagnetic activities and plasma convection and paused the progression of the storm main phase for ~ 3 hrs. Due to the sudden decrease of the dawn-to-dusk convection electric field, there was a transient period when the low-latitude ionosphere was over-shielded and experienced a brief period of dusk-to-dawn (westward) penetration electric field. The transient westward penetration electric field reversed the direction of the equatorial electrojet, and the counter electrojet was observed both in space and on the ground. The response of the ring current-R2 FAC system was delayed for ~ 6 min, and it took ~ 1 hr for the M-I system to adjust itself to the decreased plasma convection level until the low-latitude ionosphere was fully shielded again. Although the overall large-scale FACs were weakened by the negative pressure pulse, a transient, localized enhancement of downward FAC was observed near dawn, consistent with the mechanism for transmitting MHD disturbances in the M-I coupling after the negative pressure pulse. But the latitudinal location of the localized FAC enhancement differed from the model prediction, which calls further investigation of the MI coupling in response to the pressure pulse.

Acknowledgements

GL thanks Lan Jian for helpful discussion. EY was partially supported by the AFOSR (FA9550-20-1-0119) and NSF (AGS-1848730) grants. NB was partially supported by NASA Internal Scientist Funding Model on Mesoscale Dynamics.

Data Availability Statement

The OMNI data are available at <https://omniweb.gsfc.nasa.gov>. The JICA and PIUR magnetometer data are available at <https://zenodo.org/records/10823058>. The KOU and TTB magnetometer data are available at INTERMAGNET (www.intermagnet.org). The AMPERE data are available at <https://ampere.jhuapl.edu>. The Swarm data are accessible at <https://earth.esa.int/eogateway/missions/swarm/data>.

References

- Alken, P., S. Maus, A. Chulliat, P. Vigneron, O. Sirol, and G. Hulot (2015), Swarm equatorial electric field chain: First results, *Geophys. Res. Lett.*, 42, 673–680. <https://doi.org/10.1002/2014GL062658>
- Anderson, D., A. Anghel, J. Chau, and O. Veliz (2004), Daytime vertical $E \times B$ drift velocities inferred from ground-based magnetometer observations at low latitudes, *Space Weather*, 2, S11001. <https://doi.org/10.1029/2004SW000095>
- Araki, T. (1977), Global structure of geomagnetic sudden commencements, *Planet. Space Sci.*, 25, 373. [https://doi.org/10.1016/0032-0633\(77\)90053-8](https://doi.org/10.1016/0032-0633(77)90053-8)
- Araki, T. (1994). A physical model of the geomagnetic sudden commencement. *Geophysical Monograph-American Geophysical Union*, 81, 183-183. <https://doi.org/10.1029/GM081p0183>
- T. Araki, J. H. Allen (1982), Latitudinal reversal of polarization of the geomagnetic sudden commencement, *J. Geophys. Res.*, 87, 5207– 5216. <https://doi.org/10.1029/JA087iA07p05207>
- Araki, T. and H. Nagano (1988), Geomagnetic response to sudden expansions of the magnetosphere, *J. Geophys. Res.*, 93, 3983–3988. <https://doi.org/10.1029/JA093iA05p03983>
- Earle, G. D., and M. C. Kelley (1987), Spectral studies of the sources of ionospheric electric fields, *J. Geophys. Res.*, 92(A1), 213–224. <https://doi.org/10.1029/JA092iA01p00213>
- Fejer, B., C. Gonzales, D. Farley, M. Kelley, and R. Woodman (1979), Equatorial electric fields during magnetically disturbed conditions 1. The effect of the interplanetary magnetic field, *J. Geophys. Res.*, 84(A10), 5797–5802. <https://doi.org/10.1029/JA084iA10p05797>

Fejer BG, Laranja SR and Condor P (2024), Multi-process driven unusually large equatorial
 perturbation electric fields during the April 2023 geomagnetic storm. *Front. Astron. Space Sci.*
 11:1351735. <https://doi.org/10.3389/fspas.2024.1351735>

Fujita, S., T. Tanaka, T. Kikuchi, K. Fujimoto, K. Hosokawa, and M. Itonaga (2003a), A numerical
 simulation of the geomagnetic sudden commencement: 1. Generation of the field-aligned current
 associated with the preliminary impulse, *J. Geophys. Res.*, 108(A12), 1416.
<https://doi.org/10.1029/2002JA009407>

Fujita, S., T. Tanaka, T. Kikuchi, K. Fujimoto, and M. Itonaga (2003b), A numerical simulation of
 the geomagnetic sudden commencement: 2. Plasma processes in the main impulse, *J. Geophys.*
Res., 108(A12), 1417. <https://doi.org/10.1029/2002JA009763>

Fujita, S., T. Tanaka, T. Kikuchi, and S. Tsunomura (2004), A numerical simulation of a negative
 sudden impulse, *Earth Planets Space*, 56, 463–472. <https://doi.org/10.1186/BF03352499>

Fujita, S., T. Tanaka, and T. Motoba (2005), A numerical simulation of the geomagnetic sudden
 commencement: 3. A sudden commencement in the magnetosphere-ionosphere compound system,
J. Geophys. Res., 110, A11203. <https://doi.org/10.1029/2005JA011055>

Fujita, S., H. Yamagishi, K. T. Murata, M. Den, and T. Tanaka (2012), A numerical simulation of a
 negative solar wind impulse: Revisited, *J. Geophys. Res.*, 117, A09219.
<https://doi.org/10.1029/2012JA017526>

Heelis, R. A. (2004). Electrodynamics in the low and middle latitude ionosphere: A tutorial. *Journal*
of Atmospheric and Solar-Terrestrial Physics, 66(10), 825-
 838. <https://doi.org/10.1016/j.jastp.2004.01.034>

Hori, T., A. Shinbori, N. Nishitani, T. Kikuchi, S. Fujita, T. Nagatsuma, O. Troshichev, K. Yumoto,
 A. Moiseyev, and K. Seki (2012), Evolution of negative SI-induced ionospheric flows observed by

SuperDARN King Salmon HF radar, *J. Geophys. Res.*, 117, A12223,
<https://doi.org/10.1029/2012JA018093>

Jaggi, R. K., and R. A. Wolf (1973), Self-consistent calculation of the motion of a sheet of ions in the magnetosphere, *J. Geophys. Res.; Space Physics*, 78(16), 2852-2866.
<https://doi.org/10.1029/JA078i016p02852>

Kelley, M. C., J. J. Makela, J. L. Chau, and M. J. Nicolls (2003), Penetration of the solar wind electric field into the magnetosphere/ionosphere system, *Geophys. Res. Lett.*, 30, 1158.
<https://doi.org/10.1029/2002GL016321>

Morschhauser, A., Brando Soares, G., Haseloff, J., Bronkalla, O., Protásio, J., Pinheiro, K., and Matzka, J. (2017): The magnetic observatory on Tatuoca, Belém, Brazil: history and recent developments, *Geosci. Instrum. Method. Data Syst.*, 6, 367–376. <https://doi.org/10.5194/gi-6-367-2017>

Nishida, A. (1968), Coherence of geomagnetic *DP 2* fluctuations with interplanetary magnetic variations, *J. Geophys. Res.: Space Physics*, 73, 5549-5559.
<https://doi.org/10.1029/JA073i017p05549>

Richmond, A. D. (1973). Equatorial electrojet-1. Development of a model including winds and instabilities. *Journal of Atmospheric and Terrestrial Physics*, **35**(6), 1083-1103. [https://doi.org/10.1016/0021-9169\(73\)90007-x](https://doi.org/10.1016/0021-9169(73)90007-x)

Southwood, D. J. (1977), The role of hot plasma in magnetospheric convection, *J. Geophys. Res.*, 82(35), 5512–5520. <https://doi.org/10.1029/JA082i035p05512>

Southwood, D. J., and M. G. Kivelson (1990), The magnetohydrodynamic response of the magnetospheric cavity to changes in solar wind pressure, *J. Geophys. Res.*, 95, 2301–2309.
<https://doi.org/10.1029/JA095iA03p02301>

479 Tamao, T. (1964a), The structure of three-dimensional hydromagnetic waves in a uniform cold
 480 plasma, J. Geomagn. Geoelectr., 16, 89– 114, 1964a. <https://doi.org/10.5636/jgg.16.89>
 481

482 Tamao, T. (1964b), A hydromagnetic interpretation of geomagnetic SSC*, Rep. Ionos. Space Res.
 483 Jpn., 18, 16– 31.
 484

485 Yizengaw, E., M. B. Moldwin, A. Mebrahtu, B. Damtie, E. Zesta, C. E. Valladares, and P. Doherty
 486 (2011), Comparison of storm time equatorial ionospheric electrodynamics in the African and
 487 American sectors, Journal of Atmospheric and Solar-Terrestrial Physics, 73, 156-163.
 488 <https://doi.org/10.1016/j.jastp.2010.08.008>
 489

490 Yizengaw, E., M. B. Moldwin, E. Zesta, C. M. Biouele, B. Damtie, A. Mebrahtu, B. Rabiou, C. F.
 491 Valladares, and R. Stoneback (2014), The longitudinal variability of equatorial electrojet and
 492 vertical drift velocity in the African and American sector, Ann. Geophys., 32, 231–238.
 493 <https://doi.org/10.5194/angeo-32-231-2014>
 494

495 Yizengaw, E., Moldwin, M. B., Zesta, E., Magoun, M., Pradipta, R., Biouele, C. M., et al. (2016).
 496 Response of the equatorial ionosphere to the geomagnetic DP 2 current system. Geophysical
 497 Research Letters, 43(14), 7364–7372. <https://doi.org/10.1002/2016gl070090>

Solar wind-magnetosphere-ionosphere coupling and its impact on equatorial ionospheric electrodynamics during the 23 March 2023 geomagnetic storm: Effect of sudden decrease of solar wind dynamic pressure

Guan Le¹, Guiping Liu¹, and Endawoke Yizengaw², Chin-Chun Wu³, Yihua Zheng¹, Sarah Vines^{4,5}, Natalia Buzulukova^{1,6}

¹NASA Goddard Space Flight Center, Greenbelt, MD (guan.le@nasa.gov)

²The Aerospace Corporation, El Segundo, CA

³Naval Research Laboratory, Washington, DC

⁴Applied Physics Laboratory, Laurel, MD

⁵Now at Southwest Research Institute, San Antonio, TX

⁶University of Maryland, College Park, MD

Contents of this file

Figures S1

Introduction

This supporting information provides the AMPERE observations of global magnetic field perturbations and large-scale field-aligned current maps before and after the negative pressure pulse at 1440 UT on 23 March 2023.

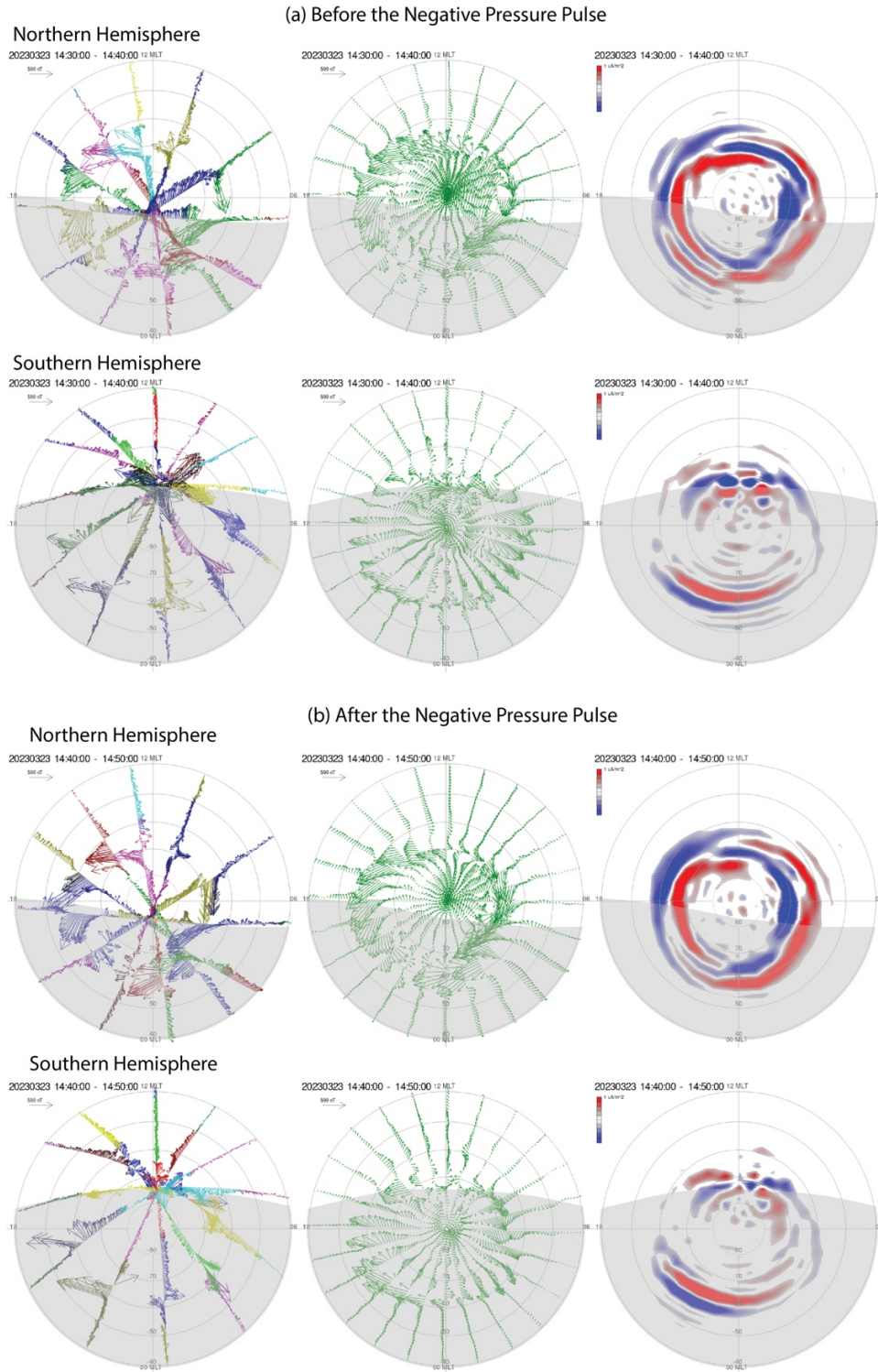


Figure S1. AMPERE global maps of observed magnetic field perturbations (left), fitted magnetic field perturbations (middle), and derived large-scale field-aligned currents patterns (right): (a) Before the negative pressure pulse 1430-1440 UT; (b) After the negative pressure pulse 1440-1450 UT.